

Coupled Eikonal problems to model cardiac reentries in Purkinje network and myocardium

Samuele Brunati^a, Michele Bucelli^a, Roberto Piersanti^{a,*}, Luca Dede^a, Christian Vergara^b

^aMOX, Laboratory of Modeling and Scientific Computing, Dipartimento di Matematica, Politecnico di Milano, Milano, Italy

^bLaBS, Laboratory of Biological Structure Mechanics, Dipartimento di Chimica, Materiali e Ingegneria Chimica, Politecnico di Milano, Milano, Italy

Abstract

We propose a novel partitioned scheme based on Eikonal equations to model the coupled propagation of the electrical signal in the His-Purkinje system and in the myocardium for cardiac electrophysiology. This scheme allows, for the first time in Eikonal-based modeling, to capture all possible signal reentries between the Purkinje network and the cardiac muscle that may occur under pathological conditions. As part of the proposed scheme, we introduce a new pseudo-time method for the Eikonal-diffusion problem in the myocardium, to correctly enforce electrical stimuli coming from the Purkinje network. We test our approach by performing numerical simulations of cardiac electrophysiology in a real biventricular geometry, under both pathological and therapeutic conditions, to demonstrate its flexibility, robustness, and accuracy.

Keywords: Cardiac electrophysiology, Purkinje network, Electrical reentries, Eikonal models, Pseudo-time method, Bundle branch block.

1. Introduction

Heart contraction is triggered by an electrical action potential propagating throughout the cardiac muscle. This process is regulated by the cardiac conduction system (CCS), schematized in Figure 1(left). The Purkinje network plays a pivotal role in driving the action potential [1, 2, 3, 4]. It is a dense network of conductive fibers, lying on the endocardium, and electrically connected to the surrounding tissue at its terminal points, called *Purkinje-muscle junctions* (PMJs). Propagation is referred to as *orthodromic* when excitation travels from the Purkinje network to the muscle, or *antidromic* when the opposite happens, as depicted in Figure 1(right). Antidromic propagation is typically absent in healthy hearts; however, it becomes relevant under diseased conditions [5, 6, 7], where *reentries*¹ in the network may occur. Therefore, incorporating both orthodromic and antidromic propagation mechanisms in computational models of cardiac electrophysiology is crucial for accurately reproducing the physical, possibly pathological, processes.

Existing cardiac computational models often lack an explicit representation of the Purkinje network, and usually surrogate it through realistic stimulation protocols based on sparse endocardial sources [9, 10, 11, 12, 13, 14, 15, 16], on space-dependent conduction velocities [17, 18, 19, 20], or on the introduction of a fast endocardial layer [21, 22, 23, 24, 25, 26, 27, 28, 29, 30, 31]. Other studies include an explicit representation of the His-Purkinje system, either rule-based [7, 32, 33, 34, 35, 36, 37, 38, 39, 40, 41, 42, 43, 44, 45, 46] or patient-specific [6, 47, 48, 49]. However, only a limited number of works have developed models that account for antidromic propagation, thus allowing a bidirectionally-coupled Purkinje-myocardium model.

*Corresponding author.

Email address: roberto.piersanti@polimi.it (Roberto Piersanti)

¹Cardiological literature generally refers to reentry as an abnormal pathway for heart signals to travel, forming a reentrant circuit, regardless of whether it involves the His-Purkinje system [8]. In this work, we focus exclusively on reentrant circuits involving the Purkinje network. With a slight misuse of terminology, we refer to such circuits simply as reentries.

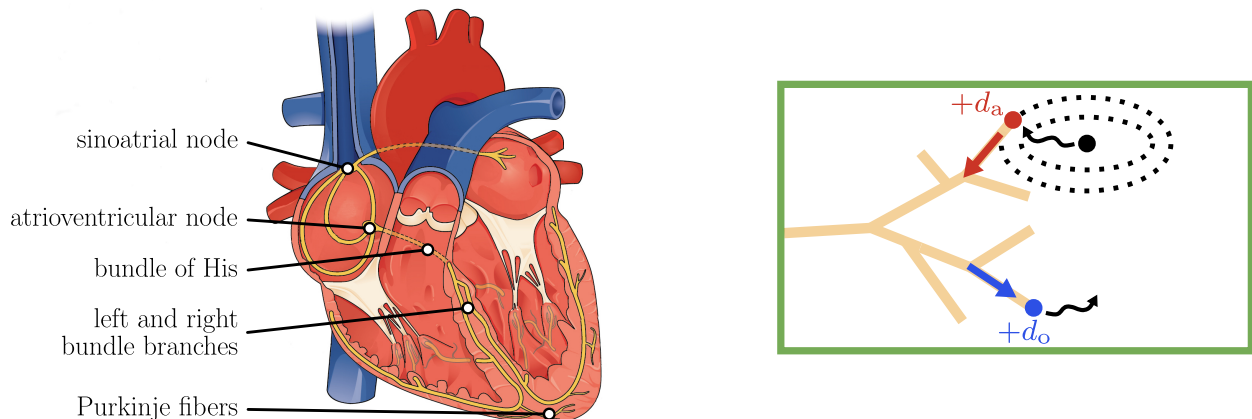


Figure 1: Left: representation of the components of the cardiac conduction system (picture adapted from https://commons.wikimedia.org/wiki/File:2018_Conduction_System_of_Heart.jpg). Focusing the attention on the ventricular electrical activity, the signal coming from the atrioventricular node (AV node) descends into the bundle of His, which divides into the right and the left bundle branches, finally branching into the Purkinje network. Right: a visualization of orthodromic (in blue) and antidromic propagation (in red) in the Purkinje network (represented in yellow) due to an intramuscular source (in black). The signal undergoes an orthodromic delay d_o before being transmitted from the Purkinje to the muscle, and an antidromic delay $d_a < d_o$ in the opposite direction.

The main issue in modeling this interplay is capturing all the possible reentries of the electrical signal between the network and the muscle. Reentrant processes have been modeled using the Monodomain equation both for network and for muscular propagation [7, 33, 36, 50, 51], or using Bidomain models [40, 42]. The work in [6] proposed an algorithm for Purkinje-muscle coupling using an *Eikonal-Eikonal* model [52], which accounts for antidromic propagation arising from possible muscular sources. However, this algorithm makes the simplifying assumption that the signal propagating from the network to the muscle cannot reenter the network, as would occur, for instance, in the presence of bundle branch blocks [33, 36, 50, 51]. Recently, a reaction-Eikonal model [23], that incorporates the Purkinje network through a monolithic approach [43, 45], yet without a detailed discussion of antidromic reentries, has been used to replicate clinical outcomes, such as for cardiac resynchronization therapy (CRT), His bundle pacing, and electrocardiograms (ECGs). In conclusion, to the best of our knowledge, no studies have been conducted using Eikonal models to address the modeling of bidirectional propagation with a discussion on reentries. Models of this kind would be useful, particularly thanks to the computational efficiency of solvers for Eikonal equations.

In this work, we present a new Eikonal-Eikonal partitioned scheme for Purkinje-muscle electrophysiology simulations, supporting both orthodromic and antidromic propagation, with a particular focus on reentries. We rely on the Eikonal model for the network and on the Eikonal-diffusion model for the muscle. The main motivations underlying our choices lie in: (i) the modularity offered by partitioned schemes, compared to the monolithic approach, allowing to solve the two problems independently using distinct solvers; and (ii) the computational advantage offered by the Eikonal models, which significantly reduce computational costs compared to the Monodomain and Bidomain ones.

We remark that Monodomain and Bidomain models have the advantage of inherently handling bidirectional propagation and PMJ delays [7], while an Eikonal-Eikonal model necessitates specific algorithms to explicitly address these interactions. In this regard, our novel algorithm improves the versatility and generality of the one proposed in [6], enabling reentries of the electrical signal between the network and the muscle. Moreover, our algorithm requires the development of a new *pseudo-time method* for the Eikonal-diffusion problem, as classic solvers would not be accurate in this coupling context.

We showcase the accuracy and the efficiency of the proposed computational framework through numerical

experiments in realistic geometries and under pathological or therapeutic conditions, such as bundle branch blocks and CRT.

This paper is organized as follows. Section 2 outlines the mathematical and numerical models employed in this work. Section 3 details the general parameters and computational setup. Section 4 presents the results of numerical simulations in various pathological scenarios. Finally, Section 5 provides a summary of the conclusions.

2. Mathematical and numerical models

In this section, we introduce the mathematical models used to describe the propagation of electrical signals within the cardiac conduction system. In the subsequent sections we examine in detail the following modeling aspects:

- the model for the activation of the His-Purkinje system through Eikonal equation;
- the model for the activation of the myocardium using the Eikonal-diffusion equation;
- the Purkinje-myocardium coupling to manage reentries between the two domains, resulting from orthodromic and antidromic propagation, employing a novel partitioned scheme for the bidirectional coupling.

2.1. Electrical activation of the Purkinje

2.1.1. Continuous problem

We use the Eikonal equation [6, 7] to describe the propagation of electrical signals within the Purkinje fibers, represented as a one-dimensional domain $\Omega_p \subset \mathbb{R}^3$ (see Figure 2(right)):

Given $\Gamma_0 \subset \partial\Omega_p$ and $u_p^0 : \Gamma_0 \rightarrow [0, T]$; find $u_p(\mathbf{x}) : \Omega_p \rightarrow [0, T]$ such that

$$\begin{cases} c_p \left| \frac{\partial u_p}{\partial s} \right| = 1 & \text{in } \Omega_p, \\ u_p = u_p^0 & \text{on } \Gamma_0, \end{cases} \quad (1)$$

where u_p represents the unknown activation times of the network, c_p is the conduction velocity, and s is the local curvilinear coordinate along the network. Γ_0 is the set of points generating the front. In healthy scenarios, Γ_0 coincides with the atrioventricular node (AV node), whereas in general it may be composed by PMJs supporting antidromic propagation.

Equation (1) provides the activation times at any point of the Purkinje network, including the Purkinje-muscle junctions (PMJs). Conduction blocks are modeled as disconnections in the network.

2.1.2. Numerical discretization: Fast Marching method

We solve the 1D Eikonal problem using the Fast Marching method (FMM), proposed for the first time in [53] to solve the pure Eikonal equation and already applied to the context of cardiac electrophysiology [7, 54, 55]. In the 1D setting, the FMM reduces to the Dijkstra's shortest path algorithm [56].

Notably, this algorithm automatically updates the activation time for those nodes in the network where a condition is prescribed (i.e. nodes belonging to Γ_0), but a signal coming from another stimulation point arrives earlier. In other words, if a stimulus is applied to a point where the solution to (1) would result in an activation earlier than the stimulus itself, then that stimulus is disregarded by the algorithm.

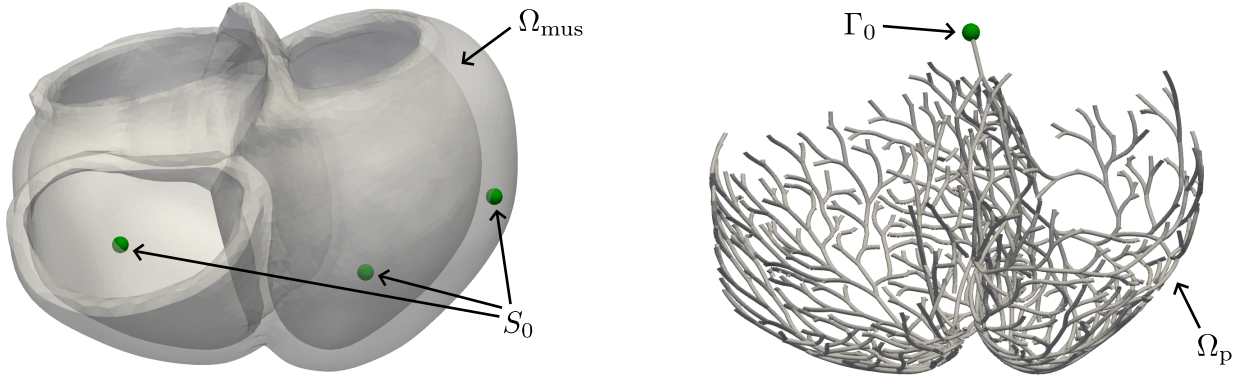


Figure 2: Ventricular myocardial domain Ω_{mus} (left) with three sources at S_0 and corresponding Purkinje domain Ω_{p} (right) with a source at Γ_0 .

2.2. Electrical activation of the myocardium

2.2.1. Continuous problem

The propagation of the electrical signal in the myocardium $\Omega_{\text{mus}} \subset \mathbb{R}^3$, see Figure 2(left), is modeled by the Eikonal-diffusion equation [13, 52]. This model is used to reconstruct the macroscopic propagation of action potential excitation wavefronts during the depolarization phase, allowing to compute the activation time as a spatial function within the myocardium.

We define the activation time $u_{\text{m}} = u_{\text{m}}(\mathbf{x})$ as the instant at which the depolarization wavefront reaches the point $\mathbf{x} \in \Omega_{\text{mus}}$. The Eikonal-diffusion model reads:

Given $u_{\text{m}}^0 \in [0, T]$ for some $\mathbf{x} \in S_0$; find $u_{\text{m}}(\mathbf{x}) : \Omega_{\text{mus}} \rightarrow [0, T]$ such that

$$\begin{cases} c_{\text{f}} \sqrt{\nabla u_{\text{m}} \cdot \boldsymbol{\Sigma} \nabla u_{\text{m}}} - \nabla \cdot (\boldsymbol{\Sigma} \nabla u_{\text{m}}) = 1 & \text{in } \Omega_{\text{mus}}, \\ (\boldsymbol{\Sigma} \nabla u_{\text{m}}) \cdot \mathbf{n} = 0 & \text{on } \partial\Omega_{\text{mus}} \setminus S_0, \\ u_{\text{m}} = u_{\text{m}}^0 & \text{on } S_0. \end{cases} \quad (2)$$

Here, \mathbf{n} is the outward directed unit vector normal to the boundary $\partial\Omega_{\text{mus}}$ of the domain Ω_{mus} , while S_0 is a portion of the physical boundary where the activation time is prescribed. Under normal propagation, S_0 coincides with the PMJs responsible for orthodromic propagation, because the signal traveling along the Purkinje network enters the muscle through these junctions. In cases of dysfunctions, additional muscular sources could be present, such as ectopic stimulation sites [6]. In (2), $\boldsymbol{\Sigma} \in \mathbb{R}^{3 \times 3}$ is the anisotropic tensor accounting for the orientation of muscular myofibers, and it is related to the conductivity tensor $\mathbf{D}(\mathbf{x})$ through the membrane capacitance C_{m} and the surface-to-volume ratio χ_{m} :

$$\boldsymbol{\Sigma} = \frac{\mathbf{D}}{\chi_{\text{m}} C_{\text{m}}} \quad \text{with} \quad \mathbf{D}(\mathbf{x}) = \sigma_{\text{f}} \mathbf{f}_0 \otimes \mathbf{f}_0 + \sigma_{\text{s}} \mathbf{s}_0 \otimes \mathbf{s}_0 + \sigma_{\text{n}} \mathbf{n}_0 \otimes \mathbf{n}_0, \quad (3)$$

where $\sigma_{\text{f}}, \sigma_{\text{s}}, \sigma_{\text{n}}$ are the conductivities along the fibers (longitudinal) \mathbf{f}_0 , the sheets (transversal) \mathbf{s}_0 , and the cross-fibers (normal) \mathbf{n}_0 directions, respectively. Accurately modeling myocardial fiber arrangement is essential to reproduce the anisotropic propagation occurring in the muscle [14, 57]. We prescribed muscular fibers, employing the strategy proposed by [14, 58], through the algorithm by Bayer et al. [57], which is a Laplace-Dirichlet rule-based method. Finally, the parameter c_{f} , uniform over the domain Ω_{mus} , is the velocity of the action potential depolarization planar wavefront along the fiber direction in an infinite cable, under the assumption of a unit surface-to-volume ratio, membrane capacitance, and conductivity [59, 60] and normalized with respect to the diffusion parameter.

The first term in the first equation of (2) is the classical Eikonal term, describing the propagation of a front in an anisotropic domain (where the anisotropy is captured by \mathbf{D}). The second term is a generalized Laplacian representing anisotropic diffusion, establishing a connection between the speed of the wavefront and its curvature. Propagation is faster when the wavefront is concave, and slower when it is convex [2, 60].

Problem (2) is very convenient from a computational standpoint, if compared to the Monodomain and the Bidomain models. Firstly, it requires solving a single steady PDE, albeit non-linear, as opposed to the Monodomain and Bidomain problems, which are time-dependent and must be coupled to ODE systems for ionic modeling [2, 52]. More importantly, the activation time, unlike the transmembrane potential, typically does not feature sharp fronts or strong gradients. Therefore, the Eikonal model does not demand for a fine spatial resolution [61, 62, 63, 64], enabling the simulation of the activation of large volumes of cardiac tissue with relatively low computational costs.

2.2.2. Numerical discretization: a novel pseudo-time method

The numerical solution of (2) requires a discretization with a proper treatment of the non-linearity. Classical non-linear solvers, such as Newton's method, typically have convergence issues in this context, due to the difficulty of finding an appropriate initial guess to problem (2) [52]. To circumvent this issue, one can numerically solve (2) by recovering the steady-state solution of the following parabolic pseudo-time problem [52, 65]:

$$\frac{\partial u_{\mathbf{m}}}{\partial t} + c_{\text{f}} \sqrt{\nabla u_{\mathbf{m}} \cdot \boldsymbol{\Sigma} \nabla u_{\mathbf{m}}} - \nabla \cdot (\boldsymbol{\Sigma} \nabla u_{\mathbf{m}}) = 1 \quad \text{in } \Omega_{\text{mus}}. \quad (4)$$

This is known as *pseudo-time* method. In (5), we propose a different version of the pseudo-time method, introduced to properly handle the Purkinje-muscle coupled propagation, since standard versions would not be accurate in the context of our new coupling algorithm, as detailed in what follows.

Starting from Equation (4), the time discretization employing a fully implicit backward differentiation formula (BDF) of order σ (say BDF σ ; $\sigma = 1, 2, \dots$), along with proper boundary and initial conditions, reads:

At each pseudo-time t^n , given $S^{n+1} \subset S_0$ and $u_{\mathbf{m}}^0 : S_0 \rightarrow \mathbb{R}$; find u^{n+1} such that

$$\left\{ \begin{array}{ll} \frac{\alpha_{\text{BDF}} u^{n+1} - u_{\text{BDF}\sigma}^n}{\Delta t} + c_{\text{f}} \sqrt{\nabla u^{n+1} \cdot \boldsymbol{\Sigma} \nabla u^{n+1}} - \nabla \cdot (\boldsymbol{\Sigma} \nabla u^{n+1}) = 1 & \text{in } \Omega_{\text{mus}}, \\ (\boldsymbol{\Sigma} \nabla u^{n+1}) \cdot \mathbf{n} = 0 & \text{on } \partial\Omega_{\text{mus}} \setminus S^{n+1}, \\ u^{n+1} = u_{\mathbf{m}}^0 & \text{on } S^{n+1}, \end{array} \right. \quad (5)$$

where $u^n \simeq u_{\mathbf{m}}(\mathbf{x}, t^n)$ is the numerical solution, $\Delta t = t^{n+1} - t^n$, while α_{BDF} and $u_{\text{BDF}\sigma}^n$ are the terms associated to the BDF σ time discretization² [66, 67]. The novelty of our approach lies in the location where Dirichlet-type conditions are imposed. Specifically, the collection of all N stimulation points $S_0 = \{\mathbf{x}_i\}_{i=1}^N$, is replaced now by S^{n+1} , containing only the subset of S_0 related to *active* stimuli. At time t^{n+1} , active stimuli are identified by:

$$\mathbf{x}_i \in S^{n+1} \iff u_{\mathbf{m}}^0(\mathbf{x}_i) < t^{n+1} \quad \text{and} \quad u_{\mathbf{m}}^0(\mathbf{x}_i) < u^n(\mathbf{x}_i). \quad (6)$$

Dirichlet-type conditions are imposed only on the stimulation points that the algorithm identifies as active, whereas inactive stimuli are disregarded. Therefore, we underline that the solution of (5) is deliberately not consistent with the continuous problem (2), since the steady-state solution only satisfies the condition $u_{\mathbf{m}} = u_{\mathbf{m}}^0$ on a subset of S_0 . Thus, (5) can be seen both as an alternative approach to Eikonal modeling of cardiac activation and as a solving methodology. A rigorous derivation of the pseudo-time-continuous counterpart to (5) is not addressed in this paper.

² α_{BDF} is a constant coefficient, while $u_{\text{BDF}\sigma}^n$ refers to the value of the function u at the current, or possibly earlier, time steps, or even a combination of them. For instance, for BDF1, $\alpha_{\text{BDF}} = 1$ and $u_{\text{BDF}\sigma}^n = u^n$, while for BDF2, $\alpha_{\text{BDF}} = 3$ and $u_{\text{BDF}\sigma}^n = 4u^n - u^{n-1}$, and so on.

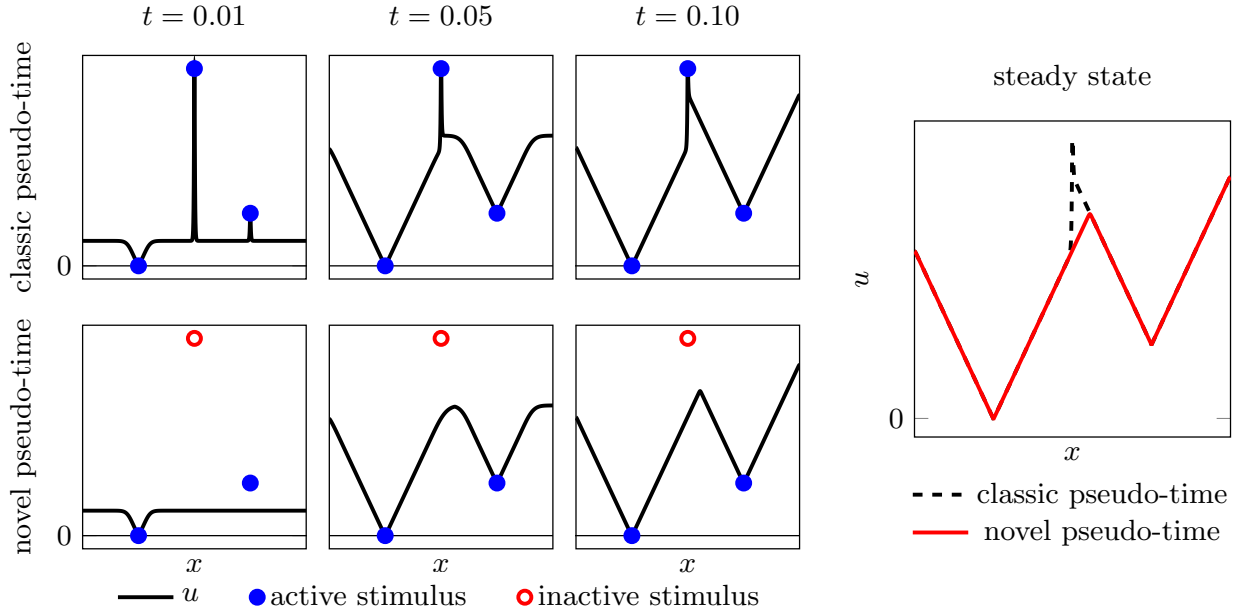


Figure 3: Numerical solution returned by the novel pseudo-time method in a one-dimensional example, compared to the classic pseudo-time method. The spatial domain is $x \in [0, L]$. Three stimuli are imposed: two are classified as active stimuli by the novel algorithm (in blue) and one as inactive (in red). At each pseudo-time step the solution is updated and stimulation points are identified as either active or inactive according to (6). Notably, the steady-state solution obtained with the classic pseudo-time method is physically meaningless, because the latest stimulus should be disregarded, as its activation time is later than the one induced by the other two.

Figure 3 helps clarifying the rationale behind the development of our novel solver. The figure compares the evolution of the solutions obtained by the classic and novel pseudo-time methods for the same set of stimuli. The novel algorithm correctly identifies one stimulus as being inactive, whereas the classic algorithm would lead to a non-physical activation delay in correspondence of that stimulus. The novel pseudo-time formulation is essential for obtaining physically meaningful solutions during the coupling with the Purkinje network.

For the linearization and space discretization of (5) we use the standard Newton method and the Galerkin-Finite Element method [68].

2.3. Purkinje-muscle fully coupled problem

To address the coupling between the problems (1) and (2), we introduce the following functionals, which map the stimuli to the corresponding activation times both in the myocardium and in the Purkinje network:

$$\mathcal{E} : S_0 \mapsto u_m \quad \mathcal{P} : \Gamma_0 \mapsto u_p.$$

Our starting point is the coupling strategy presented in [6]. The interface conditions of the coupled problem are related to the continuity of the activation times u_p and u_m at the PMJs. The latter are classified into:

- *antidromic PMJs*, which are activated by the front coming from the muscle, and delay the signal by d_a before transmitting it to the Purkinje network.
- *orthodromic PMJs*, which are activated by the front coming from the AV node or emerging in the network due to antidromic propagation, and delay the signal by d_o before transmitting it to the myocardium.

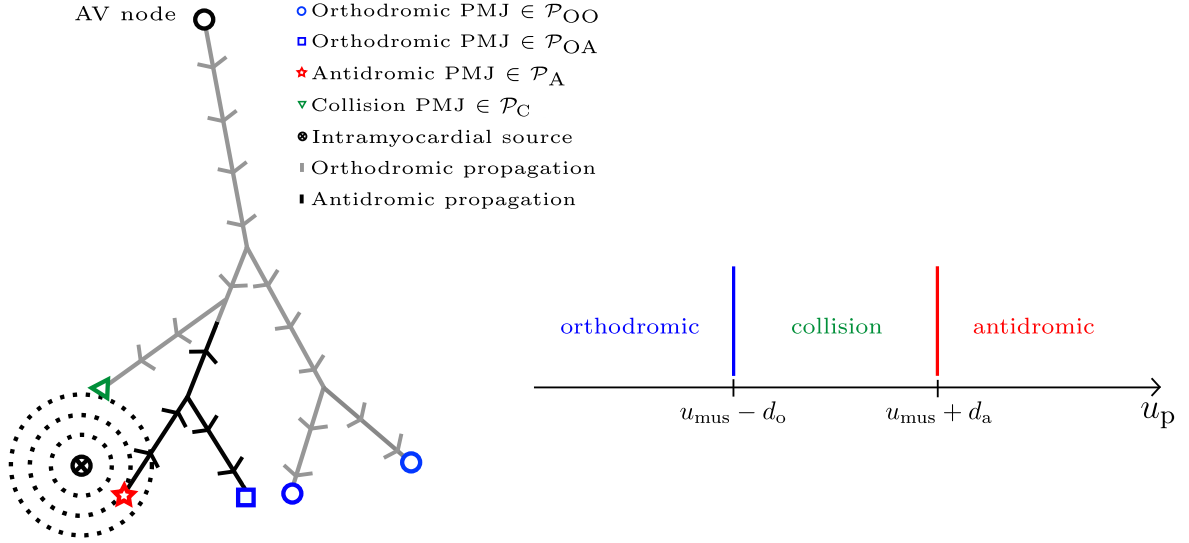


Figure 4: Purkinje-muscle junctions (PMJs) classification in presence of opposite wavefronts propagating between the Purkinje network and the myocardium. Right: graphical representation of the function $\mathbf{classify_pmjs}(pmjs, u_p, u_m)$, defined in Algorithm 2. In the notation, AV node stands for atrioventricular node. Two types of orthodromic PMJs are introduced: \mathcal{P}_{OO} is the collection of orthodromic PMJs activated by an electrical signal coming from the AV node, while \mathcal{P}_{OA} is the collection of orthodromic PMJs activated by a signal coming from an antidromic PMJ.

- *collision PMJs*³, which arise when the muscular and the network wavefronts collide at the PMJ itself, so they are neither orthodromic nor antidromic. This is possible due to the presence of a delay at the PMJs.

Figure 4 schematically illustrates the different types of PMJs resulting from orthodromic and antidromic propagation.

We propose hereafter Algorithm 1, designed to overcome the limitations of [6]. The latter made the assumption that the antidromic activation of the PMJs is induced exclusively by the muscular sources. This implies that the muscular pathways that activate the network could only be generated by the muscular sources. In other words, with the algorithm of [6], a signal originating from the AV node and entering the muscle through a PMJ cannot reenter the network. Conversely, our approach is able to account for potential occurrence of reentries. Algorithm 1 allows for an excitation front to originate at the AV node, enter the muscle through a PMJ and subsequently reenter the Purkinje network at a different PMJ. This is achieved by incorporating subiterations in the algorithm, thus repeatedly solving the two Eikonal problems and exchanging information at the PMJs until the maximum number of iterations is reached, and it is made possible by the use of the new pseudo-time method described in Section 2.2.2. We fix the number of iterations to $N = N_{\max}$, although this can be straightforwardly improved through a suitable stopping criterion.

The PMJs classification, showed in Figure 4, is updated through the function $\mathbf{classify_pmjs}$, illustrated in Algorithm 2.

³This is a new category, introduced in this work, to speed up and correctly classify PMJs in Algorithm 1.

Algorithm 1 1D Eikonal - 3D Eikonal strong coupling

```
1: Notation:  $AVN$  = atrioventricular node,  $\mathcal{M}$  = collection of the possible muscular sources,  $pmj_{o_i}$  =  $i$ -th ortho-  
dromic PMJ,  $pmj_{a_i}$  =  $i$ -th antidromic PMJ,  $u_m$  = activation time in the muscle,  $u_p$  = activation time in the  
His-Purkinje system,  $pmj_o/pmj_a/pmj_c$  = orthodromic/antidromic/collision PMJs  
2: Input:  $AVN, \mathcal{M}, N_{\max}$   
3: Output:  $u_p, u_m, pmjs$   
4:  $u_p \leftarrow \mathcal{P}(\{AVN\})$   
5:  $pmjs \leftarrow$  get Purkinje-muscle junctions (PMJs)  
6: for ( $i < N_{\max}$ ) do  
7:    $u_m \leftarrow \mathcal{E}(\mathcal{M} \cup \{pmj_{o_1}, pmj_{o_2}, \dots, pmj_{o_N}\})$   
8:    $[pmj_o, pmj_a, pmj_c] \leftarrow \text{classify\_pmjs}(pmjs, u_p, u_m)$   
9:    $u_p \leftarrow \mathcal{P}(\{AVN, pmj_{a_1}, pmj_{a_2}, \dots, pmj_{a_M}\})$   
10:   $[pmj_o, pmj_a, pmj_c] \leftarrow \text{classify\_pmjs}(pmjs, u_p, u_m)$   
11: end for
```

Algorithm 2 Function `classify_pmjs(pmjs, u_p, u_m)`

```
1: for ( $pmj:pmjs$ ) do  
2:   if ( $u_p[pmj] \geq u_m[pmj] + \text{antidromic\_delay}$ ) then  
3:      $PmjType[pmj] = \text{"Antidromic"}$   
4:   else if ( $u_p[pmj] \leq u_m[pmj] - \text{orthodromic\_delay}$ ) then  
5:      $PmjType[pmj] = \text{"Orthodromic"}$   
6:   else  
7:      $PmjType[pmj] = \text{"Collision"}$   
8:   end if  
9: end for
```

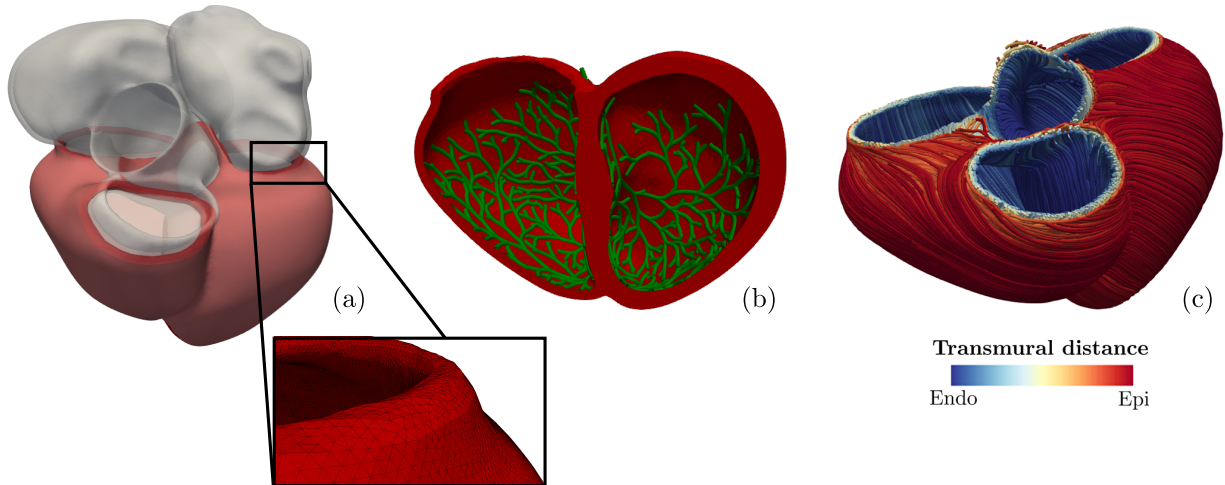


Figure 5: (a) Real biventricular geometry reconstructed from four-chamber heart of a patient [62], with tetrahedral mesh discretization. (b) A section of the ventricles with the generated Purkinje network. (c) Muscular fibers visualization. The fiber field is visualized as streamlines, colored according to the transmural distance, going from the endocardium (Endo, in blue) to the epicardium (Epi, in red).

3. Simulations setting

In this section, we briefly introduce the general setting of the numerical simulations that will be presented in Section 4. Section 3.1 describes the computational domains considered for the 3D ventricular geometry and the 1D Purkinje network, while Section 3.2 summarizes the common parameter settings for all the numerical simulations. Finally, Section 3.3 is dedicated to the computational environment adopted to implement the algorithms and to perform the simulations.

3.1. Computational domains

The 3D cardiac computational domain, depicted in Figure 5, is a patient-specific human biventricular geometry, reconstructed from a computed tomography (CT) scan of a patient. This geometry is obtained from a publicly available cohort of four-chamber hearts presented in [62]. The mesh was segmented from a CT scan of the heart of an 83-years-old male who was recruited for a CRT upgrade following heart failure. Since this is not a healthy heart, it exhibits certain non-physiological features such as muscular hypertrophy and myocardial thickening. Moreover, endocardial structures, such as papillary muscles, are not included in the segmentation.

The extraction of the ventricular portion and the volumetric mesh generation (with an average edge length of 0.8 mm) was performed using `vmtk`⁴ and the methods described in [69]. The main characteristics of the obtained mesh are summarized in Table 1.

Incorporating a patient-specific His-Purkinje system represents a distinct challenge, since currently no imaging technique is able to reconstruct a patient-specific network for human hearts. We used the open-source Python library `fractal-tree`⁵ to generate the 1D Purkinje network [41]. This approach employs a semi-automatic algorithm based on a fractal law, designed to generate a network standing on an endocardial surface discretized by triangles, mimicking the tree structure of the Purkinje itself. An example of generated network is reported in Figure 5(b). The absence of endocardial structures in the considered 3D geometries prevents an accurate reconstruction of the network, allowing only to capture its principal features. Some significant elements, particularly the moderator band in the right ventricle, have been omitted.

⁴<http://www.vmtk.org/>

⁵<https://github.com/fsahli/fractal-tree>

element shape	tetrahedra
#elements	5'268'810
#nodes(DoFs)	927'097
aspect ratio	1.57 ± 0.53
scaled jacobian	0.63 ± 0.14
average cell diameter	0.927 mm
min cell diameter	0.377 mm
max cell diameter	1.365 mm

Table 1: Characteristics of the 3D mesh used in numerical simulations. Aspect ratio and scaled jacobian are two mesh quality metrics, defined as in [70], indicating that the mesh has acceptable regularity.

Description	Parameter	Reference
Stimulation sites and shape		
Conduction block sites		
Conductivity values	$\sigma_f = 1.00 \times 10^{-4} \text{ m}^2/\text{s}$	[14]
	$\sigma_s = 0.44 \times 10^{-4} \text{ m}^2/\text{s}$	
	$\sigma_n = 0.11 \times 10^{-4} \text{ m}^2/\text{s}$	
Depolarization velocity of the myocardium	$c_f = 60 \text{ s}^{-1/2}$	[14]
Conduction velocity of the Purkinje	$c_p = 4 \text{ m/s}$	[71, 7]
Orthodromic PMJ delay	$d_o = 10 \times 10^{-3} \text{ s}$	[7]
Antidromic PMJ delay	$d_a = 2 \times 10^{-3} \text{ s}$	[7]

Table 2: Summary of the main physical parameter used in the numerical simulations.

3.2. Simulation parameters

Table 2 reports the main physical parameters useful for solving the Eikonal model. Following [14], we select the conductivity values in the myocardium to obtain the conduction velocities of 0.6 m/s in the fiber direction, 0.4 m/s in the sheet direction and 0.2 m/s in the normal direction [14, 71]. We selected the conduction velocity in the Purkinje fibers to be 4 m/s [27, 71, 48]. At the PMJs, the signal experiences a delay of 10 ms – 15 ms for orthodromic propagation and a shorter delay of 2 ms – 3 ms for antidromic propagation [7].

Finally, pointwise stimuli in the muscle are applied at the PMJs, while spherical stimuli of radius 0.5 mm are imposed in correspondence of possible ectopic or artificial stimuli. The placement of muscular sources and possible conduction blocks is evaluated case-by-case and passed as input through their point coordinates.

3.3. Simulation environment

The numerical framework presented in Section 2 has been implemented in `lifex` [72, 73, 74]⁶, a high-performance C++ finite element library for cardiovascular modeling, based on `deal.II` [75, 76, 77].

Simulations have been performed using the HPC facilities of the Mathematics Department at Politecnico di Milano, running on one node with 20 cores 4x Xeon E5-2640 v4 (2.4GHz) with 384GB of RAM. Running $N_{\max} = 3$ iterations⁷ of Algorithm 2 takes less than 2 hours.

4. Numerical results

This section is dedicated to present numerical results from electrophysiology simulations using the model framework introduced in Section 2 and based on the setting presented in Section 3. Computational simulations offer a valuable tool for medical decision-making. This ability to simulate different scenarios with

⁶<https://lifex.gitlab.io>

⁷The choice $N_{\max} = 3$, in Algorithm 1, is done to balance reliable results with reduced computational time.

	$\mu \pm \sigma$ (ms)	TAT	EAT
T-H	64.0 ± 14.8	140.7	27.6
T-WPW	56.9 ± 17.3	120.5	-30.0
T-LBBB	86.0 ± 26.4	174.0	31.1
T-CRT	83.8 ± 25.6	173.4	31.1

Table 3: Average activation time (μ), standard deviation (σ), total activation time (TAT) and earliest activation time (EAT) of the myocardium in the four test scenarios. All the times refer to $t = 0$ ms, when the signal starts from the atrioventricular node.

	T-H	T-WPW	T-LBBB	T-CRT
OO	522	490	305	305
OA	0	27	142	108
A	0	1	23	39
C	9	13	61	79

Table 4: PMJs (#531) classification returned by Algorithm 1 in all the test cases. OO=orthodromic activated by AV node; OA=orthodromic activated by antidromic PMJs; A=antidromic; C=collision.

relative computational ease, without intervening on the patient, represents, in perspective, a notable application [2, 3, 23, 45, 78]. We consider four test (T) scenarios, illustrating both healthy and pathological propagation:

- T-H: healthy propagation. The atrioventricular node represents the unique stimulation point for ventricular activation and only orthodromic propagation is present [4].
- T-WPW: Wolff-Parkinson-White syndrome. A pathological scenario characterized by an intramuscular source in addition to His-Purkinje activation [5, 6, 7].
- T-LBBB: complete left bundle branch block. A pathological scenario characterized by a complete conduction block in the left bundle branch [5, 45].
- T-CRT: cardiac resynchronization therapy. A model therapeutical scenario, which combines both features of the previous test cases, introducing multiple intramuscular sources and a complete left bundle branch block [79, 45].

Figures 6 and 7 compare the activation times and the PMJs classification of the four test cases, respectively. The two figures are completed by Tables 3 and 4, which collect synthetical indices related to the activation maps and to the PMJs classification.

4.1. T-H: healthy propagation

We present a simulation characterized by healthy propagation, which will be used as a baseline for comparisons with the pathological scenarios. Figure 6(b,c) shows the resulting activation map. Only orthodromic propagation is present, following His-Purkinje activation, which takes approximately 30 ms, in alignment with the values recorded in-vivo [27]. The sub-endocardial layer is the first portion of the muscle to activate, with the signal progressively spreading throughout the myocardium and transmurally towards the epicardium. The propagation follows an apico-basal pattern, favored by the scarce presence of Purkinje fibers near the ventricular bases. The total ventricular activation times are reported to be around 80 ms – 100 ms in healthy patients [48, 80]. The latest activation time, recorded in Table 4, is slightly elevated, likely due to the inclusion of the valvular plane in the geometry and to muscle thickening caused by the patient’s hypertrophy.

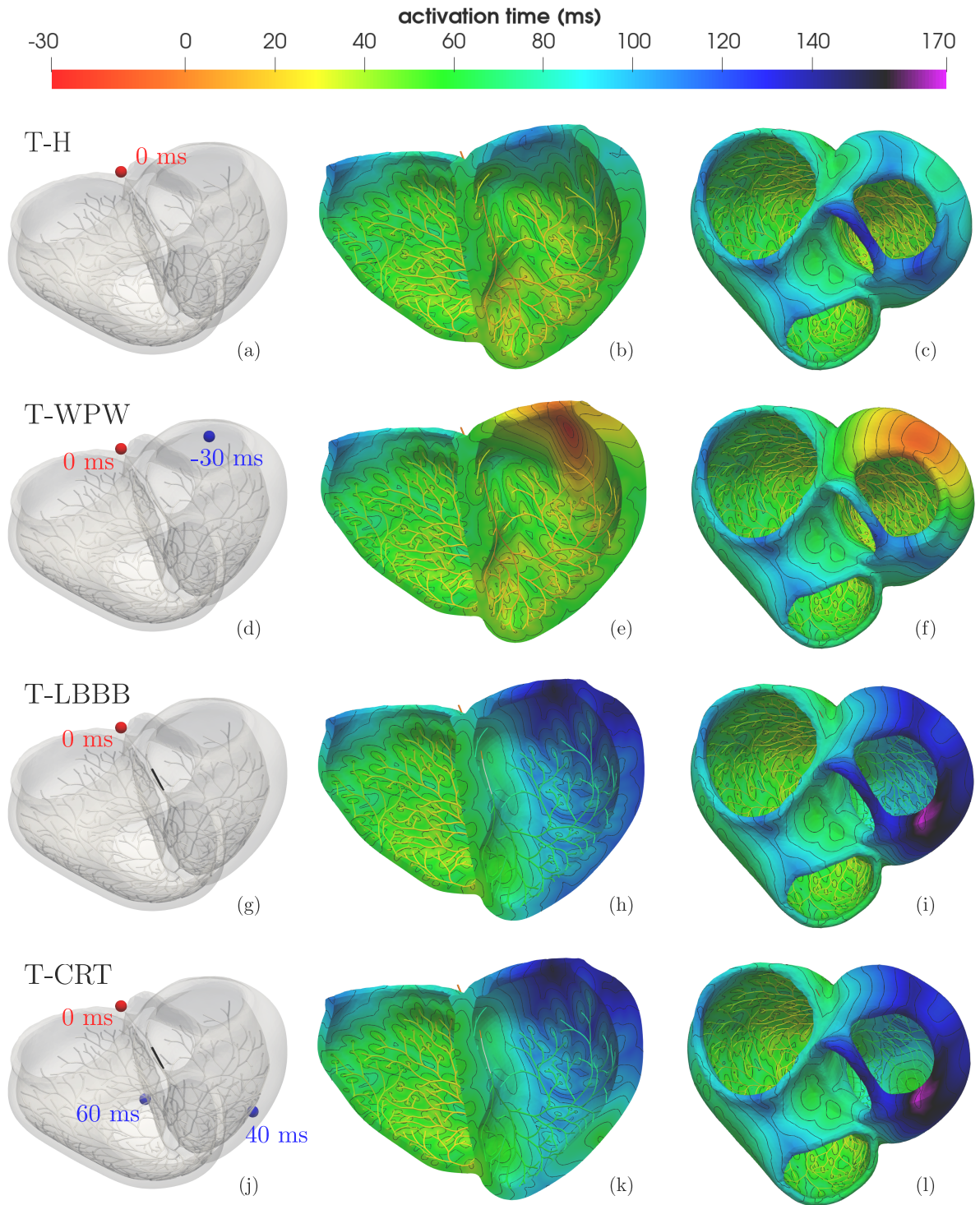


Figure 6: Comparative view of the four scenarios: T-H, T-WPW, T-LBBB, T-CRT. First column: simulation setup; second column: activation map of a section of the biventricular geometry; third column: activation map from top view. Isochrones are spaced 10ms apart. The bundle branch block is highlighted in black in figures (g) and (j). The activation time of the atrioventricular node (AV node) is taken as reference starting at 0 ms.

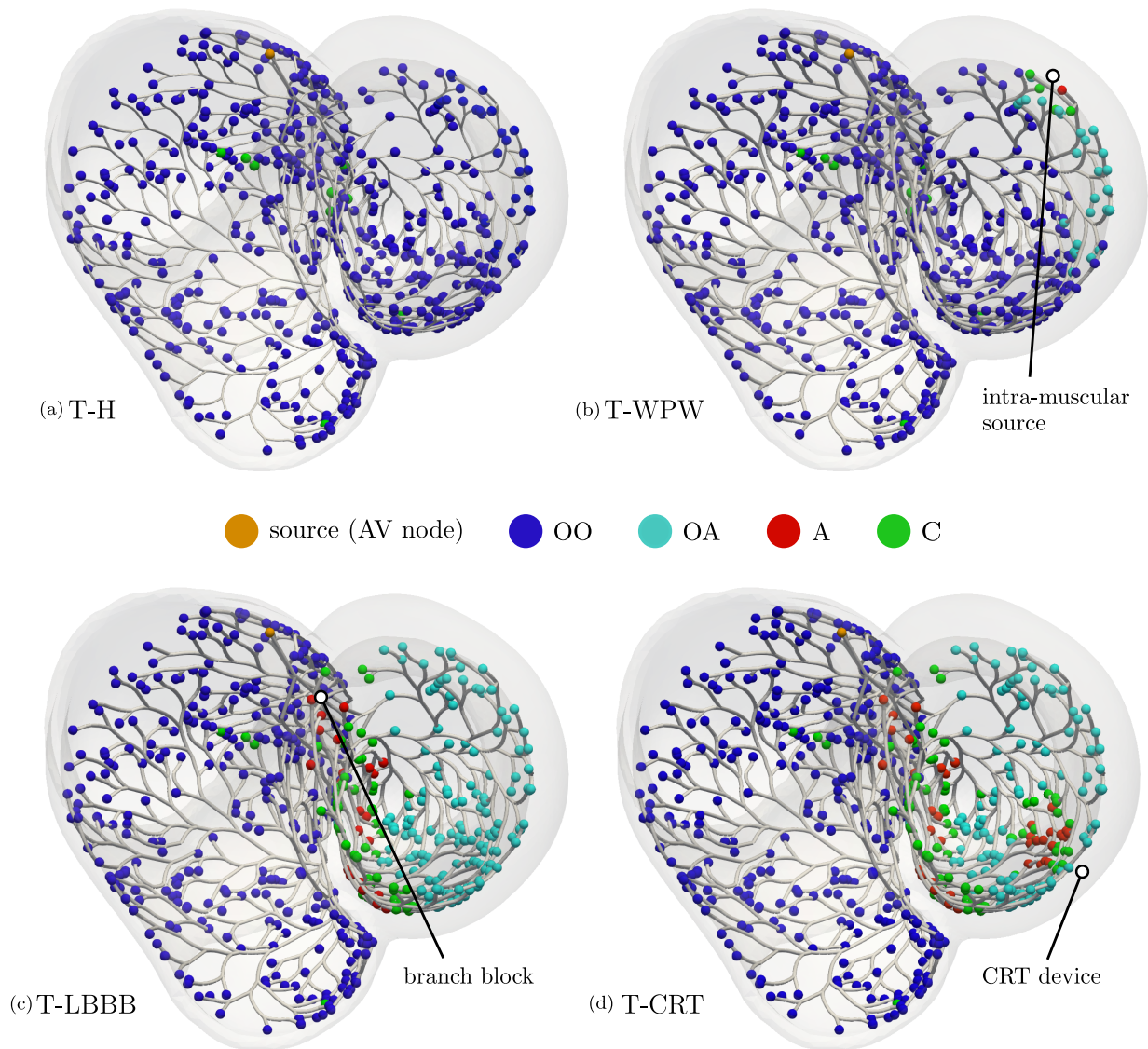


Figure 7: Graphical visualization of the Purkinje-muscle junctions (PMJs) classification in the four test cases. PMJs are represented as spheres of different colors according to their type: source (orange), orthodromic activated by AV node (OO, blue), orthodromic activated by antidromic propagation (OA, cyan), antidromic (A, red), collision (C, green). Non-orthodromic PMJs are localized close to anomalous sources.

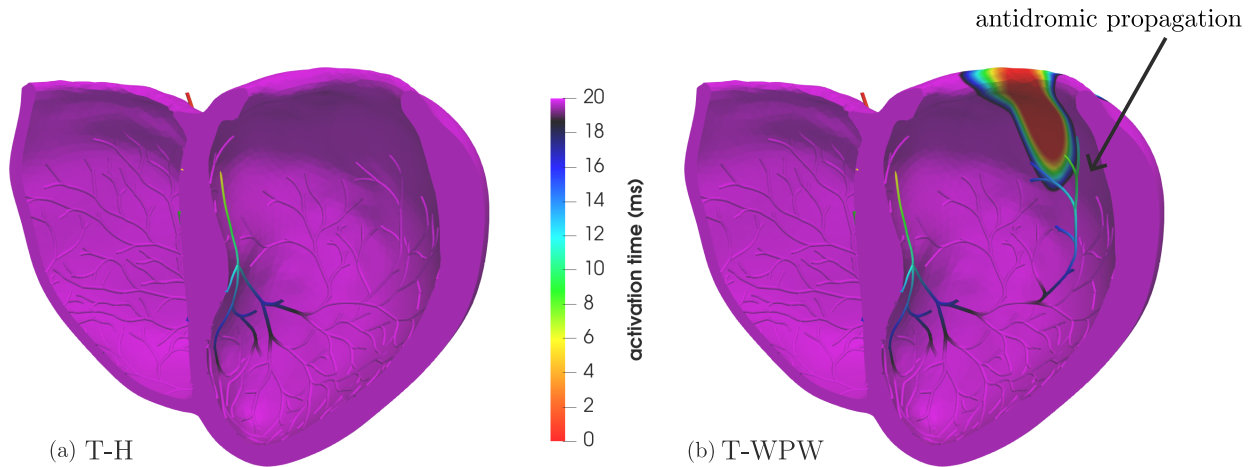


Figure 8: Comparison between T-H (a) and T-WPW (b). The activation time scale was saturated in the range 0 ms – 20 ms in order to highlight the identification, in the pathological scenario, of two opposite fronts propagating in the Purkinje network. The effect of antidromic propagation due to the intramuscular source is visible in T-WPW, while only orthodromic propagation is present in T-H.

4.2. T-WPW: Wolff-Parkinson-White syndrome

The Wolff-Parkinson-White (WPW) syndrome is a pathology characterized by the presence of an accessory pathway between the left atrium and the left ventricle, named bundle of Kent [81, 82, 83]. Since we only consider a ventricular geometry, we follow the modeling approach proposed in [6], which surrogates the effect of WPW syndrome on the ventricles by introducing an intramuscular source at the termination of the Kent bundle. This induces a pre-excitation of the left ventricle.

The simulation pacing setup is shown in Figure 6(d). A muscular source was placed in the posterolateral portion, near the basal plane, of the left ventricular myocardium, consistently with in-vivo observations of the location of the Kent bundle [6, 84]. Here, a spherical stimulus with radius 0.5 mm was applied at time $t = -30$ ms to replicate the pre-excitation of the muscle, considering that the activation of the AV node starts later at $t = 0$ ms, which is used as reference time across all the scenarios.

Figure 6(e,f) shows the the resulting activation map. A front propagating through the muscle is clearly observed before the signal starts to propagate through the network, causing the pre-excitation of the upper posterolateral portion of the left ventricle. At the orthodromic PMJs, focal activation is still visible. Away from the muscular source, all the PMJs are orthodromic, while near it antidromic or collision PMJs arise, as we can see in Figure 7(b).

Figure 8 reports a comparison between T-H and T-WPW, highlighting the effects of antidromic propagation. We observe that, in the presence of only orthodromic activation, in Figure 8(a), the signal reaches only the three branches diverging from the main bundle of the Purkinje network. Meanwhile, thanks to the pre-excitation of the muscle starting at $t = -30$ ms, the signal enters the network antidromically in Figure 8(b). Here, two wavefronts are distinguishable in opposite directions. Close to the ectopic stimulation point, all the types of PMJs are present: antidromic, collision and orthodromic activated by antidromic propagation (OA-labelled PMJs).

4.3. T-LBBB: complete left bundle branch block

The second pathological scenario considered is a complete left bundle branch block (LBBB). The latter consists in the interruption of the electric signal propagation in a segment of the left branch, resulting in an alteration of ventricular synchrony [5, 85].

The atrioventricular node was stimulated as in the healthy case at time $t = 0$ ms (see Section 4.1). A conduction block is located along a segment of the left bundle branch, shown in black in Figure 6(g).

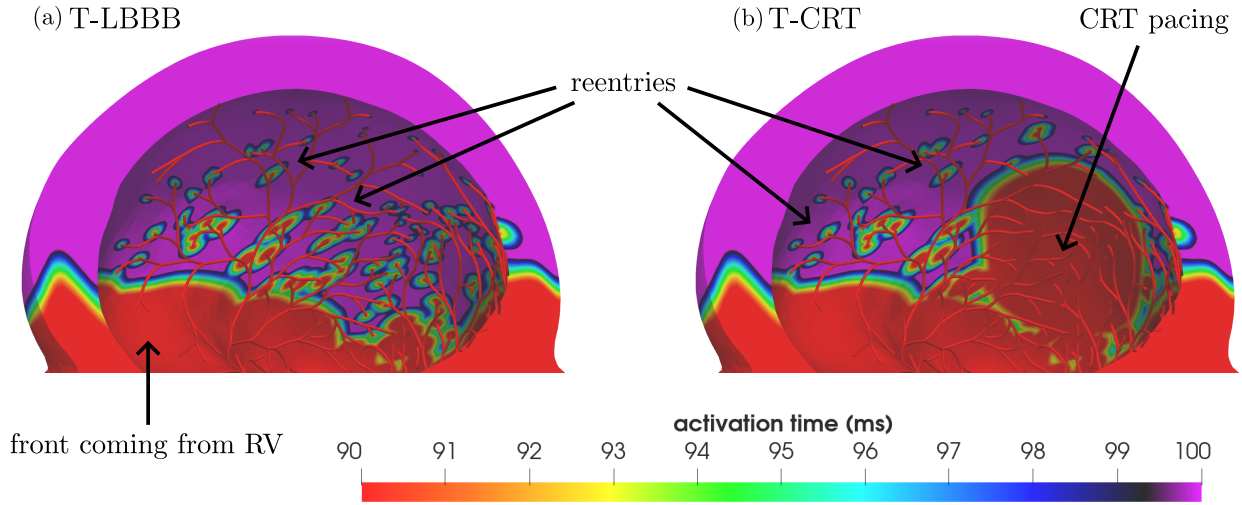


Figure 9: A zoom on the reentries of the electrical signal in the muscle in T-LBBB (a) and T-CRT (b): the muscular wavefront coming from the healthy right ventricle (RV) traverses the interventricular septum and antidromically activates the Purkinje network in the left ventricle, where propagation is interrupted in correspondence of the branch block. Purkinje fibers conduct at higher velocity so that the signal is able to re-emerge orthodromically from PMJs (reentries highlighted in picture). To show the fronts, the color scales have been properly saturated.

The total activation time is 174 ms, as reported in Table 3 and shown in Figure 6(h,i). The signal originates from the atrioventricular node and travels through the His bundle. At the conduction block, the signal path in the left branch is interrupted, continuing toward the ventricle solely through the right branch. In Figure 6(h), we can notice how the right ventricle undergoes normal orthodromic activation, while the signal in the left ventricle arrives later. The wavefront reaches the left ventricle through the interventricular septum, see Figure 6(h), coherently with what is observed in patients with complete branch blocks. Consequently, impulses enter in the left branch of network antidromically. Figure 7(c) shows that the conduction block determines the presence of antidromic PMJs near the interventricular septum. Moreover, no orthodromic PMJs activated by the signal coming from the AV node (OO-labelled PMJs) are present in the left ventricle. In contrast, we see many OA-labelled PMJs, which result from a signal that has entered the network antidromically from the muscle and, due to the higher conduction velocity in the Purkinje fibers, is able to reemerge orthodromically from a different PMJ. A high number of OA PMJs is confirmed also by Table 4.

Figure 9(a) displays the activation map for the time frame 90 ms – 100 ms, highlighting the reentry propagation from the muscle to the network. The higher transmission velocity in the network causes the signal to re-emerge again in the muscle. In Figure 9(a), a primary front is coming from the right ventricle, overcome by the stimuli arriving from the terminations of the left network. We emphasize that our new proposed Algorithm 1 made it possible to numerically observe this reentry effect. In contrast, the methodologies outlined in [6] would not be able to capture such reentries, providing a less biophysically accurate solution.

4.4. T-CRT: cardiac resynchronization therapy

The last presented scenario combines the two sources of antidromic propagation, both the conduction block and the muscular source, into a single simulation, showcasing the versatility of the algorithm for Purkinje-muscle coupling. This test case aims to simulate the effects of cardiac resynchronization therapy (CRT) in presence of a complete left bundle branch block. CRT is a treatment that involves biventricular pacing to help restoring the normal rhythm and timing of the heartbeat [45, 78, 79]. This involves implanting electrodes in the heart to produce artificial stimuli that compensate for the propagation imbalance caused

by a particular pathology. Typically, one lead is placed at the apex of the right ventricle, and another on the free wall midway up the left ventricle [1, 79, 86, 87]. The effect of artificial pacing is modeled by defining two appropriate epicardial stimuli [45, 78].

Figure 6(j) resumes the initial setup of the simulation. A stimulus at time $t = 0$ ms is imposed at the AV node, with a complete conduction block located as in T-LBBB (see Section 4.3). Two additional spherical stimuli are imposed in order to mimic the two leads of CRT. Activation at these points occurs at time $t = 60$ ms and $t = 40$ ms, consisting of spherical stimuli with radius 0.5 mm. Notice that this is an arbitrary choice, as is their location, which usually corresponds to the termination of two cardiac veins. The correct positioning and timing may vary a lot from patient to patient and are evaluated in clinical practice on individual specifics.

The biventricular activation map is depicted in Figure 6(k,l). The CRT lead in the right ventricle has, on purpose, a higher activation time than the one ensured by orthodromic propagation, in order to verify that it produces no effect. Indeed, the novel pseudo-time method, proposed in Section 2.2.2, correctly operates in this situation. Conversely, the lead in the left ventricle produces a stimulus that impacts the solution, as shown in Figure 6(k,l). This is even more visible in Figure 9(b), where the artificial pacing is evident, along with the signal entering the network via antidromic PMJs. Several wavefronts are present in the muscle: one main front, which comes from the interventricular septum, and one produced by the CRT lead, but also many pointwise stimuli at PMJs due to reentries. The right ventricle activates normally, while the left ventricle shows alterations compared to the healthy case. The latter are partially compensated by the artificial pacing, ensuring better activation of the lateral wall of the left ventricle. Figure 9 also provides a comparison between T-LBBB (a) and T-CRT (b): the anterolateral portion of the left ventricle is activated thanks to CRT. In T-CRT, in addition to the antidromic and collision PMJs in correspondence to the interventricular septum, further PMJs of these types are present near the CRT device, as depicted in Figure 7(d). Moreover, many orthodromic PMJs activated due to antidromic propagation (OA type) are visible in the free wall of the left ventricle, consistently with the reentry effect.

5. Conclusions

In this paper, we studied the interaction of the electrical excitation in the cardiac muscle and the Purkinje network using Eikonal equations, focusing on modeling electrical reentries. We proposed a novel Eikonal-diffusion pseudo-time method capable of correctly imposing active stimuli in the muscle while discarding inactive ones. Furthermore, we introduced a novel Purkinje-muscle coupling partitioned scheme (Algorithm 1) that effectively manages possible reentries between the two domains by iteratively computing activation times and exchanging information at the interface, represented by the PMJs. Building on and extending the work presented in [6], we addressed its limitations, achieving improved versatility and accuracy.

While this work primarily focused on methodological and modeling aspects, we also performed numerical simulations in realistic pathological and therapeutic scenarios. The results underscore the critical role of the Purkinje network and highlight the importance of accurately capturing electrical reentries to better reproduce the pathophysiological processes. The numerical simulations showcased the accuracy, flexibility and robustness of our algorithm, successfully handling arbitrary combinations of Purkinje network, stimulation setups and conduction blocks.

A promising direction for future work is to rigorously define the continuous formulation of the pseudo-time-discrete problem (5), which is not consistent with (2) and implicitly introduces a novel notion of solution, whose properties warrant further investigation. Additionally, our numerical experiments relied on Purkinje networks reconstructed through rule-based algorithms, rather than patient-specific. However, thanks to the modularity of the proposed scheme, the latter can be included straightforwardly. Finally, investigating pathological scenarios from an electro-mechanical perspective may provide deeper insights into their effects on cardiac function.

Acknowledgements

M.B., R.P. and L.D. received support from the project PRIN2022, MUR, Italy, 2023–2025 202232A8AN “Computational modeling of the heart: from efficient numerical solvers to cardiac digital twins”. R.P. has also received support from the INdAM GNCS project CUP E53C23001670001 “Mathematical models and numerical methods for the construction of cardiac digital twins”. C.V. has been partially supported by: i) the European Union-Next Generation EU, Mission 4, Component 1, CUP: D53D23018770001, under the research project MUR PRIN22-PNRR n.P20223KSS2, “Machine learning for fluid structure interaction in cardiovascular problems: efficient solutions, model reduction, inverse problems”, ii) the Italian Ministry of Health within the PNC PROGETTO HUB LIFE SCIENCE - DIAGNOSTICA AVANZATA (HLS-DA) “INNOVA”, PNCE3-2022-23683266–CUP: D43C22004930001, within the “Piano Nazionale Complementare Ecosistema Innovativo della Salute” - Codice univoco investimento: PNCE3-2022-23683266; iii) the Italian research project MUR PRIN22 n.2022L3JC5T “Predicting the outcome of endovascular repair for thoracic aortic aneurysms: analysis of fluid dynamic modeling in different anatomical settings and clinical validation”; iv) Italian Ministry of Health within the project “CAL.HUB.RIA” - CALABRIA HUB PER RICERCA INNOVATIVA ED AVANZATA. Code: T4-AN-09, CUP: F63C22000530001. M.B., R.P., L.D. and C.V. acknowledge their membership to INdAM group GNCS - Gruppo Nazionale per il Calcolo Scientifico (National Group for Scientific Computing, Italy). M.B. and R.P. acknowledge the INdAM GNCS project CUP E53C23001670001. M.B., R.P. and L.D. acknowledge the “Dipartimento di Eccellenza 2023-2027”, MUR, Italy, Dipartimento di Matematica, Politecnico di Milano.

Declaration of competing interest

All the authors declare that they have no known competing financial interests or personal relationships that could have appeared to influence the work reported in this paper.

CRedit authorship contribution statement

S. Brunati: Conceptualization, Methodology, Software, Simulation, Data curation, Formal analysis, Investigation, Visualization, Writing – original draft, Writing – review & editing. **M. Bucelli:** Conceptualization, Methodology, Software, Formal analysis, Investigation, Visualization, Writing – original draft, Writing – review & editing. **R. Piersanti:** Conceptualization, Methodology, Formal analysis, Investigation, Visualization, Writing – original draft, Writing – review & editing. **L. Dede’:** Supervision, Funding acquisition, Project administration, Writing – review & editing. **C. Vergara:** Conceptualization, Supervision, Funding acquisition, Project administration, Writing – original draft, Writing – review & editing.

References

- [1] P. A. Iaizzo, Handbook of cardiac anatomy, physiology, and devices, Springer Science & Business Media, 2010.
- [2] A. Quarteroni, A. Manzoni, C. Vergara, The cardiovascular system: mathematical modelling, numerical algorithms and clinical applications, *Acta Numerica* 26 (2017) 365–590.
- [3] A. Quarteroni, L. Dede’, A. Manzoni, C. Vergara, Mathematical modelling of the human cardiovascular system: data, numerical approximation, clinical applications, Vol. 33, Cambridge University Press, 2019.
- [4] M. A. Bagni, D. Brambilla, L. Catacuzzeno, M. Catalano, M. Contini, R. Crescenzo, M. D’Amelio, C. Faggio, M. P. Gallo, E. Grasselli, R. Gulino, G. Leanza, R. Maccarone, A. Michelucci, D. A. Ragozzino, I. Sirangelo, C. Veronesi, *Fisiologia*, Edises, 2023.
- [5] M. Romanò, *Testo-atlante di elettrocardiografia pratica: Approccio clinico ragionato all’elettrocardiogramma*, Springer Science & Business Media, 2010.
- [6] S. Palamara, C. Vergara, D. Catanzariti, E. Faggiano, C. Pangrazzi, M. Centonze, F. Nobile, M. Maines, A. Quarteroni, Computational generation of the Purkinje network driven by clinical measurements: the case of pathological propagations, *International Journal for Numerical Methods in Biomedical Engineering* 30 (12) (2014) 1558–1577.
- [7] C. Vergara, M. Lange, S. Palamara, T. Lassila, A. F. Frangi, A. Quarteroni, A coupled 3D-1D numerical Monodomain solver for cardiac electrical activation in the myocardium with detailed Purkinje network, *Journal of Computational Physics* 308 (2016) 218–238.

- [8] D. Fleischmann, T. Pop, J. De Bakker, Reentry mechanism within the His-Purkinje system in man during extrasystolic stimulation of the right ventricle, in: *Cardiac Pacing: Diagnostic and Therapeutic Tools*, Springer, 1976, pp. 194–204.
- [9] E. J. Vigmond, M. Hughes, G. Plank, L. J. Leon, Computational tools for modeling electrical activity in cardiac tissue, *Journal of Electrocardiology* 36 (2003) 69–74.
- [10] D. Nickerson, N. Smith, P. Hunter, New developments in a strongly coupled cardiac electromechanical model, *EP Europace* 7 (s2) (2005) S118–S127.
- [11] D. Keller, R. Kalayciyan, O. Dössel, G. Seemann, Fast creation of endocardial stimulation profiles for the realistic simulation of body surface ECGs, in: *World Congress on Medical Physics and Biomedical Engineering*, September 7–12, 2009, Munich, Germany: Vol. 25/4 Image Processing, Biosignal Processing, Modelling and Simulation, Biomechanics, Springer, 2010, pp. 145–148.
- [12] M. J. Bishop, G. Plank, R. A. Burton, J. E. Schneider, D. J. Gavaghan, V. Grau, P. Kohl, Development of an anatomically detailed mri-derived rabbit ventricular model and assessment of its impact on simulations of electrophysiological function, *American Journal of Physiology-Heart and Circulatory Physiology* 298 (2) (2010) H699–H718.
- [13] A. Quarteroni, T. Lassila, S. Rossi, R. Ruiz-Baier, Integrated heart—coupling multiscale and multiphysics models for the simulation of the cardiac function, *Computer Methods in Applied Mechanics and Engineering* 314 (2017) 345–407.
- [14] R. Piersanti, P. C. Africa, M. Fedele, C. Vergara, L. Dede', A. F. Corno, A. Quarteroni, Modeling cardiac muscle fibers in ventricular and atrial electrophysiology simulations, *Computer Methods in Applied Mechanics and Engineering* 373 (2021) 113468.
- [15] F. Regazzoni, M. Salvador, P. C. Africa, M. Fedele, L. Dede', A. Quarteroni, A cardiac electromechanical model coupled with a lumped-parameter model for closed-loop blood circulation, *Journal of Computational Physics* 457 (2022) 111083.
- [16] P. C. Africa, M. Salvador, P. Gervasio, L. Dede', A. Quarteroni, A matrix-free high-order solver for the numerical solution of cardiac electrophysiology, *Journal of Computational Physics* 478 (2023) 111984.
- [17] T. P. Usyk, I. J. LeGrice, A. D. McCulloch, Computational model of three-dimensional cardiac electromechanics, *Computing and Visualization in Science* 4 (2002) 249–257.
- [18] S. Göktepe, E. Kuhl, Electromechanics of the heart: a unified approach to the strongly coupled excitation-contraction problem, *Computational Mechanics* 45 (2010) 227–243.
- [19] N. A. Trayanova, Whole-heart modeling: applications to cardiac electrophysiology and electromechanics, *Circulation Research* 108 (1) (2011) 113–128.
- [20] M. Sermesant, R. Chabiniok, P. Chinchapatnam, T. Mansi, F. Billet, P. Moireau, J.-M. Peyrat, K. Wong, J. Relan, K. Rhode, M. Ginks, P. Lambiase, H. Delingette, M. Sorine, C. A. Rinaldi, D. Chapelle, R. Razavi, N. Ayache, Patient-specific electromechanical models of the heart for the prediction of pacing acute effects in CRT: a preliminary clinical validation, *Medical Image Analysis* 16 (1) (2012) 201–215.
- [21] M. Kotikanyadanam, S. Göktepe, E. Kuhl, Computational modeling of electrocardiograms: A finite element approach toward cardiac excitation, *International Journal for Numerical Methods in Biomedical Engineering* 26 (5) (2010) 524–533.
- [22] B. Baillargeon, N. Rebelo, D. D. Fox, R. L. Taylor, E. Kuhl, The Living Heart project: a robust and integrative simulator for human heart function, *European Journal of Mechanics-A/Solids* 48 (2014) 38–47.
- [23] A. Neic, F. O. Campos, A. J. Prassl, S. A. Niederer, M. J. Bishop, E. J. Vigmond, G. Plank, Efficient computation of electrograms and ECGs in human whole heart simulations using a reaction-Eikonal model, *Journal of Computational Physics* 346 (2017) 191–211.
- [24] A. W. Lee, U. C. Nguyen, O. Razeghi, J. Gould, B. S. Sidhu, B. Sieniewicz, J. Behar, M. Mafi-Rad, G. Plank, F. W. Prinzen, C. A. Rinaldi, K. Vernooy, S. A. Niederer, A rule-based method for predicting the electrical activation of the heart with cardiac resynchronization therapy from non-invasive clinical data, *Medical Image Analysis* 57 (2019) 197–213.
- [25] K. Gillette, M. A. Gsell, A. J. Prassl, E. Karabelas, U. Reiter, G. Reiter, T. Grandits, C. Payer, D. Štern, M. Urschler, J. D. Bayer, C. M. Augustin, A. Neic, T. Pock, E. J. Vigmond, G. Plank, A framework for the generation of digital twins of cardiac electrophysiology from clinical 12-leads ECGs, *Medical Image Analysis* 71 (2021) 102080.
- [26] K. Gillette, M. A. Gsell, M. Strocchi, T. Grandits, A. Neic, M. Manninger, D. Scherr, C. H. Roney, A. J. Prassl, C. M. Augustin, E. J. Vigmond, G. Plank, A personalized real-time virtual model of whole heart electrophysiology, *Frontiers in Physiology* 13 (2022) 907190.
- [27] G. Del Corso, R. Verzicco, F. Viola, A fast computational model for the electrophysiology of the whole human heart, *Journal of Computational Physics* 457 (2022) 111084.
- [28] M. Fedele, R. Piersanti, F. Regazzoni, M. Salvador, P. C. Africa, M. Bucelli, A. Zingaro, L. Dede', A. Quarteroni, A comprehensive and biophysically detailed computational model of the whole human heart electromechanics, *Computer Methods in Applied Mechanics and Engineering* 410 (2023) 115983.
- [29] R. Piersanti, F. Regazzoni, M. Salvador, A. F. Corno, L. Dede', C. Vergara, A. Quarteroni, 3D-0D closed-loop model for the simulation of cardiac biventricular electromechanics, *Computer Methods in Applied Mechanics and Engineering* 391 (2022) 114607.
- [30] M. Bucelli, A. Zingaro, P. C. Africa, I. Fumagalli, L. Dede', A. Quarteroni, A mathematical model that integrates cardiac electrophysiology, mechanics, and fluid dynamics: Application to the human left heart, *International Journal for Numerical Methods in Biomedical Engineering* 39 (3) (2023) e3678.
- [31] E. Zappon, M. Salvador, R. Piersanti, F. Regazzoni, L. Dede', A. Quarteroni, An integrated heart-torso electromechanical model for the simulation of electrophysiological outputs accounting for myocardial deformation, *Computer Methods in Applied Mechanics and Engineering* 427 (2024) 117077.
- [32] S. Abboud, O. Berenfeld, D. Sadeh, Simulation of high-resolution QRS complex using a ventricular model with a fractal conduction system. Effects of ischemia on high-frequency QRS potentials., *Circulation Research* 68 (6) (1991) 1751–1760.
- [33] O. Berenfeld, J. Jalife, Purkinje-muscle reentry as a mechanism of polymorphic ventricular arrhythmias in a 3-dimensional

- model of the ventricles, *Circulation Research* 82 (10) (1998) 1063–1077.
- [34] E. J. Vigmond, C. Clements, Construction of a computer model to investigate sawtooth effects in the Purkinje system, *IEEE transactions on biomedical engineering* 54 (3) (2007) 389–399.
- [35] T. Ijiri, T. Ashihara, T. Yamaguchi, K. Takayama, T. Igarashi, T. Shimada, T. Namba, R. Haraguchi, K. Nakazawa, A procedural method for modeling the Purkinje fibers of the heart, *The Journal of Physiological Sciences* 58 (7) (2008) 481–486.
- [36] K. Ten Tusscher, A. V. Panfilov, Modelling of the ventricular conduction system, *Progress in Biophysics and Molecular Biology* 96 (1-3) (2008) 152–170.
- [37] D. Romero, R. Sebastian, B. H. Bijmens, V. Zimmerman, P. M. Boyle, E. J. Vigmond, A. F. Frangi, Effects of the Purkinje system and cardiac geometry on biventricular pacing: a model study, *Annals of Biomedical Engineering* 38 (2010) 1388–1398.
- [38] R. Sebastian, V. Zimmerman, D. Romero, D. Sanchez-Quintana, A. F. Frangi, Characterization and modeling of the peripheral cardiac conduction system, *IEEE Transactions on Medical Imaging* 32 (1) (2012) 45–55.
- [39] R. M. Bordas, K. Gillow, D. Gavaghan, B. Rodríguez, D. Kay, A Bidomain model of the ventricular specialized conduction system of the heart, *SIAM Journal on Applied Mathematics* 72 (5) (2012) 1618–1643.
- [40] E. Behradfar, A. Nygren, E. J. Vigmond, The role of Purkinje-myocardial coupling during ventricular arrhythmia: a modeling study, *PLoS one* 9 (2) (2014) e88000.
- [41] F. S. Costabal, D. E. Hurtado, E. Kuhl, Generating Purkinje networks in the human heart, *Journal of Biomechanics* 49 (12) (2016) 2455–2465.
- [42] M. Landajuela, C. Vergara, A. Gerbi, L. Dede', L. Formaggia, A. Quarteroni, Numerical approximation of the electromechanical coupling in the left ventricle with inclusion of the Purkinje network, *International Journal for Numerical Methods in Biomedical Engineering* 34 (7) (2018) e2984.
- [43] M. Strocchi, A. W. Lee, A. Neic, J. Bouyssier, K. Gillette, G. Plank, M. K. Elliott, J. Gould, J. M. Behar, B. Sidhu, V. Mehta, M. J. Bishop, E. J. Vigmond, C. A. Rinaldi, S. A. Niederer, His-bundle and left bundle pacing with optimized atrioventricular delay achieve superior electrical synchrony over endocardial and epicardial pacing in left bundle branch block patients, *Heart Rhythm* 17 (11) (2020) 1922–1929.
- [44] M. Peirlinck, F. S. Costabal, J. Yao, J. Guccione, S. Tripathy, Y. Wang, D. Ozturk, P. Segars, T. Morrison, S. Levine, E. Kuhl, Precision medicine in human heart modeling: perspectives, challenges, and opportunities, *Biomechanics and Modeling in Mechanobiology* 20 (2021) 803–831.
- [45] M. Strocchi, K. Gillette, A. Neic, M. K. Elliott, N. Wijesuriya, V. Mehta, E. J. Vigmond, G. Plank, C. A. Rinaldi, S. A. Niederer, Comparison between conduction system pacing and cardiac resynchronization therapy in right bundle branch block patients, *Frontiers in Physiology* 13 (2022) 1011566.
- [46] S. Reza, B. Kovarovic, D. Bluestein, Assessing post-tavr cardiac conduction abnormalities risk using an electromechanically coupled beating heart, *Biomechanics and Modeling in Mechanobiology* (2024) 1–17.
- [47] O. Camara, A. Pashaei, R. Sebastian, A. F. Frangi, Personalization of fast conduction Purkinje system in Eikonal-based electrophysiological models with optical mapping data, in: *Statistical Atlases and Computational Models of the Heart: First International Workshop, STACOM 2010, and Cardiac Electrophysiological Simulation Challenge, CESC 2010, Held in Conjunction with MICCAI 2010, Beijing, China, September 20, 2010. Proceedings 1*, Springer, 2010, pp. 281–290.
- [48] S. Palamara, C. Vergara, E. Faggiano, F. Nobile, An effective algorithm for the generation of patient-specific Purkinje networks in computational electrocardiology, *Journal of Computational Physics* 283 (2015) 495–517.
- [49] J. Camps, L. A. Berg, Z. J. Wang, R. Sebastian, L. L. Riebel, R. Doste, X. Zhou, R. Sachetto, J. Coleman, B. Lawson, V. Grau, K. Burrage, A. Bueno-Orovio, R. Weber dos Santos, B. Rodriguez, Digital twinning of the human ventricular activation sequence to clinical 12-lead ECGs and magnetic resonance imaging using realistic Purkinje networks for in silico clinical trials, *Medical Image Analysis* 94 (2024) 103108.
- [50] E. J. Vigmond, B. D. Stuyvers, Modeling our understanding of the His-Purkinje system, *Progress in Biophysics and Molecular Biology* 120 (1-3) (2016) 179–188.
- [51] E. J. Vigmond, J. Bouyssier, J. Bayer, M. Haïssaguerre, H. Ashikaga, On the nature of delays allowing anatomical re-entry involving the Purkinje network: a simulation study, *EP Europace* 23 (Supplement_1) (2021) i71–i79.
- [52] P. Colli Franzone, L. F. Pavarino, S. Scacchi, *Mathematical cardiac electrophysiology*, Vol. 13, Springer, 2014.
- [53] J. A. Sethian, Fast marching methods, *SIAM review* 41 (2) (1999) 199–235.
- [54] E. Pernod, M. Sermesant, E. Konukoglu, J. Relan, H. Delingette, N. Ayache, A multi-front Eikonal model of cardiac electrophysiology for interactive simulation of radio-frequency ablation, *Computers & Graphics* 35 (2) (2011) 431–440.
- [55] T. Grandits, K. Gillette, A. Neic, J. Bayer, E. Vigmond, T. Pock, G. Plank, An inverse Eikonal method for identifying ventricular activation sequences from epicardial activation maps, *Journal of Computational Physics* 419 (2020) 109700.
- [56] E. W. Dijkstra, A note on two problems in connexion with graphs, in: *Edsger Wybe Dijkstra: His Life, Work, and Legacy*, Springer, 2022, pp. 287–290.
- [57] J. D. Bayer, R. C. Blake, G. Plank, N. A. Trayanova, A novel rule-based algorithm for assigning myocardial fiber orientation to computational heart models, *Annals of biomedical engineering* 40 (2012) 2243–2254.
- [58] P. C. Africa, R. Piersanti, M. Fedele, L. Dede', A. Quarteroni, lifex-fiber: an open tool for myofibers generation in cardiac computational models, *BMC Bioinformatics* 24 (1) (2023) 143.
- [59] P. Colli Franzone, L. Guerri, Spreading of excitation in 3D models of the anisotropic cardiac tissue. i. Validation of the Eikonal model, *Mathematical Biosciences* 113 (2) (1993) 145–209.
- [60] P. Colli Franzone, L. Guerri, M. Pennacchio, B. Taccardi, Spread of excitation in 3D models of the anisotropic cardiac tissue. ii. Effects of fiber architecture and ventricular geometry, *Mathematical Biosciences* 147 (2) (1998) 131–171.
- [61] P. Colli Franzone, L. F. Pavarino, S. Scacchi, Reduced macroscopic models: The Monodomain and Eikonal models,

- Mathematical Cardiac Electrophysiology (2014) 123–148.
- [62] M. Strocchi, C. M. Augustin, M. A. Gsell, E. Karabelas, A. Neic, K. Gillette, O. Razeghi, A. J. Prassl, E. J. Vigmond, J. M. Behar, J. Gould, B. Sidhu, C. A. Rinaldi, M. J. Bishop, G. Plank, S. A. Niederer, A publicly available virtual cohort of four-chamber heart meshes for cardiac electro-mechanics simulations, *PloS one* 15 (6) (2020) e0235145.
 - [63] S. Stella, F. Regazzoni, C. Vergara, L. Dede', A. Quarteroni, A fast cardiac electromechanics model coupling the Eikonal and the nonlinear mechanics equations, *Mathematical Models and Methods in Applied Sciences* 32 (08) (2022) 1531–1556.
 - [64] L. Gander, R. Krause, M. Weiser, F. Sahli Costabal, S. Pezzuto, On the accuracy of Eikonal approximations in cardiac electrophysiology in the presence of fibrosis, in: *International Conference on Functional Imaging and Modeling of the Heart*, Springer, 2023, pp. 137–146.
 - [65] A. Quarteroni, L. Formaggia, A. Veneziani, *Complex systems in biomedicine*, Springer, 2006.
 - [66] A. Quarteroni, R. Sacco, F. Saleri, *Numerical mathematics*, Vol. 37, Springer Science & Business Media, 2010.
 - [67] D. Forti, L. Dedè, Semi-implicit bdf time discretization of the navier–stokes equations with vms-les modeling in a high performance computing framework, *Computers & Fluids* 117 (2015) 168–182.
 - [68] R. Piersanti, R. Bradley, S. Y. Alid, A. Quarteroni, L. Dede, N. A. Trayanova, Defining myocardial fiber bundle architecture in atrial digital twins, *arXiv preprint arXiv:2410.11601* (2024).
 - [69] M. Fedele, A. Quarteroni, Polygonal surface processing and mesh generation tools for the numerical simulation of the cardiac function, *International Journal for Numerical Methods in Biomedical Engineering* 37 (4) (2021) e3435.
 - [70] C. Stimpson, C. Ernst, P. Knupp, P. Pébay, D. Thompson, *The Verdict library reference manual*, Sandia National Laboratories Technical Report 9 (6) (2007) 8.
 - [71] I. Caverio, H. Holzgrefe, Internodal conduction pathways: revisiting a century-long debate on their existence, morphology, and location in the context of 2023 best science, *Advances in Physiology Education* 47 (4) (2023) 838–850.
 - [72] P. C. Africa, lifex: A flexible, high performance library for the numerical solution of complex finite element problems, *SoftwareX* 20 (2022) 101252.
 - [73] P. C. Africa, R. Piersanti, F. Regazzoni, M. Bucelli, M. Salvador, M. Fedele, S. Pagani, L. Dede', A. Quarteroni, lifex-ep: a robust and efficient software for cardiac electrophysiology simulations, *BMC Bioinformatics* 24 (1) (2023) 389.
 - [74] M. Bucelli, The lifex library version 2.0, *arXiv preprint arXiv:2411.19624* (2024).
 - [75] W. Bangerth, R. Hartmann, G. Kanschat, deal.II—a general-purpose object-oriented finite element library, *ACM Transactions on Mathematical Software (TOMS)* 33 (4) (2007) 24–es.
 - [76] D. Arndt, W. Bangerth, D. Davydov, T. Heister, L. Heltai, M. Kronbichler, M. Maier, J.-P. Pelteret, B. Turcksin, D. Wells, The deal.II finite element library: Design, features, and insights, *Computers & Mathematics with Applications* 81 (2021) 407–422.
 - [77] D. Arndt, W. Bangerth, M. Feder, M. Fehling, R. Gassmüller, T. Heister, L. Heltai, M. Kronbichler, M. Maier, P. Munch, J.-P. Pelteret, S. Sticko, B. Turcksin, D. Wells, The deal.II library, version 9.4, *Journal of Numerical Mathematics* 30 (3) (2022) 231–246.
 - [78] A. W. Lee, C. M. Costa, M. Strocchi, C. A. Rinaldi, S. A. Niederer, Computational modeling for cardiac resynchronization therapy, *Journal of Cardiovascular Translational Research* 11 (2018) 92–108.
 - [79] F. Leyva, S. Nisam, A. Auricchio, 20 years of cardiac resynchronization therapy, *Journal of the American College of Cardiology* 64 (10) (2014) 1047–1058.
 - [80] D. Durrer, R. T. Van Dam, G. Freud, M. J. Janse, F. L. Meijler, R. C. Arzbacher, Total excitation of the isolated human heart, *Circulation* 41 (6) (1970) 899–912.
 - [81] W. C. Sealy, J. J. Gallagher, E. L. Pritchett, The surgical anatomy of Kent bundles based on electrophysiological mapping and surgical exploration, *The Journal of Thoracic and Cardiovascular Surgery* 76 (6) (1978) 804–815.
 - [82] S. M. Al-Khatib, E. L. Pritchett, Clinical features of Wolff-Parkinson-White syndrome, *American Heart Journal* 138 (3) (1999) 403–413.
 - [83] S. Mittal, Atrioventricular accessory path: (the Kent bundle), in: *Insights into Electrocardiograms with MCQs*, Springer, 2023, pp. 97–110.
 - [84] B. F. Waller, C. M. Orr, J. D. Slack, C. A. Pinkerton, J. V. Tassel, T. Peters, B. Waller, Anatomy, histology, and pathology of coronary arteries: A review relevant to new interventional and imaging techniques-part iv, *Clinical Cardiology* 15 (9) (1992) 675–687.
 - [85] J. H. McAnulty, S. H. Rahimtoola, Bundle branch block, *Progress in Cardiovascular Diseases* 26 (4) (1984) 333–354.
 - [86] C. Butter, A. Auricchio, C. Stellbrink, M. Schlegl, E. Fleck, W. Hörsch, E. Huvelle, J. Ding, A. Kramer, P. T. in Congestive Heart Failure II Study Group, W. Hörsch, E. Huvelle, J. Ding, A. Kramer, Should stimulation site be tailored in the individual heart failure patient?, *The American Journal of Cardiology* 86 (9) (2000) K144–K151.
 - [87] P. T. Mortensen, P. Sogaard, H. Mansour, J. Ponsonaille, D. Gras, A. Lazarus, W. Reiser, C. Alonso, C. M. Linde, M. Lunati, B. Kramm, E. M. Harrison, Sequential biventricular pacing: evaluation of safety and efficacy, *Pacing and Clinical Electrophysiology* 27 (3) (2004) 339–345.